ELSEVIER

Catalysis Today 68 (2001) 111–118

CATALYSIS TODAY

www.elsevier.com/locate/cattod

NH_3 desorption and decomposition behavior on microporous hollandite-type hydrous manganese oxide

Zheng-Ming Wang*, Satoko Tezuka, Hirofumi Kanoh

Aquamaterial Separation Technology RG, Marine Resources and Environment Institute, National Institute of Advanced Industrial Science and Technology, 2217-14 Hayashi-cho, Takamatsu-shi, Kagawa 761-0395, Japan

Abstract

In order to figure out the catalytic property of hollandite-type hydrous manganese oxide (H-Hol) to remove NH_3, the desorption and decomposition properties of NH_3 from NH_3-chemically adsorbed H-Hol were examined and these properties and NH_3 adsorptivity were compared with those of other manganese oxides and a de-NO_x catalyst. It was found that the presence of NO accelerates the oxidation of NH_3 to form N_2 at a lower temperature. Comparison of NH_3 pulse reaction in a flow containing NO on H-Hol with those on a high surface area-manganese oxide and a commercial de-NO_x catalyst shows that H-Hol has the greatest N_2 production, but less selectivity to form N_2. H-Hol has a comparable amount of the strong H^+ sites with the high surface area manganese oxide, which have relationship with NH_3 decomposition.

Keywords: H-Hol; NH_3; Adsorptivity; Decomposition

1. Introduction

Hollandite-type hydrous manganese oxide (H-Hol) or OMS-2 by designation of Suib et al. [1] is one of representative porous manganese oxides, which contains (2 × 2) one-dimensional tunnel structure surrounded by inter-linking of edge-shared MnO_6 octahedral units [1–4]. The crystalline opening of the rectangular tunnel structure of H-Hol is estimated as 0.46 nm. However, the effective pore opening for gas adsorption and ion sieving adsorption in liquid phase is around 0.26–0.265 and 0.282 nm, respectively [5,6]. Because of its excellent ion-sieving property, application of H-Hol as a cathode material for rechargeable battery and as an inorganic exchanger has been widely studied [1,6–8]. However, the catalytic properties of H-Hol and other porous manganese oxides have not been sufficiently studied so far [3,9–11], partly because of a confined pore entrance and intra-pore spaces due to the blocking effect from both negative O^{2-} ions and the presence of counter cations.

Although large molecules can be excluded to the extra-pores, NH_3 can be selectively adsorbed into the intra-pores of H-Hol under co-existence of water, indicating that H-Hol can be a selective killer for odor NH_3 [5]. Since NH_3 molecules are strongly stabilized in the tunnel structure of H-Hol with an adsorption energy larger than 200 kJ/mol [12], a preliminary research shows that the NH_3 adsorbed can only be desorbed in a large amount as a form of N_2 at the same time that the structural transformation occurs on increasing temperature. In order to examine the catalytic property of H-Hol to remove NH_3, it is thus, essential to examine the desorption property of NH_3

* Corresponding author. Tel.: +81-878693574; fax: +81-878693550.
E-mail address: zm_wang@aist.go.jp (Z.-M. Wang).

0920-5861/01/$ – see front matter
PII: S0920-5861(01)00297-8

from NH_3-adsorbed H-Hol. In this research, desorption property of NH_3-adsorbed H-Hol was studies under the presence of various gas atmosphere, from which a condition for catalytic decomposition of NH_3 has been derived. The NH_3 adsorption, and catalytic decomposition properties were also compared with another manganese oxide having large surface area and a standard commercial de-NO_x catalyst.

2. Experimental

2.1. Materials and characterization

H-Hol was synthesized by a hydrothermal reaction whose detailed procedure had been reported otherwise [13]. Potassium-type hollandite (K-Hol) was obtained by treatment of H-Hol in 0.1 M KOH solution at room temperature for 5 days, followed by subsequent washing with distilled water and drying at 343 K for one day. In order to prepare a manganese oxide with high surface area (HMnO), a spinel-type manganese oxide, Mg_2MnO_4, was treated in 0.5 M HCl for 10 days, followed by washing with distilled water and drying at 323 K for one night [14,15]. A commercial de-NO_x catalyst, V_2O_5/TiO_2 (VTiO), for selective reduction of NO using NH_3 as a reductant was supplied from Nikki Universal Co. Ltd.

The porosity of each catalyst was determined by low-temperature N_2 adsorption at 77 K using a commercial volumetric equipment (Autosorb-1, YUASA Co. Ltd.). The crystal structure of each catalyst was confirmed by X-ray diffractometer (RINT 1200, Rigaku), the measurement by which was carried out from 3 to 70° at a scanning speed of 0.02°/min in a temperature/humidity controllable chamber. Thermal gravimetric (TG) properties and differential thermal analysis (DTA) of the catalysts were carried out by TG-DTA 2000 system (Mac Science Co. Ltd.) from room temperature to 1273 K at a ramp rate of 10 K/min. A commercial α-Al_2O_3 product was used as the reference material.

2.2. NH_3 adsorption and desorption

NH_3 adsorption on each catalyst was measured by both a static volumetric method and a dynamic pulse injection method. A first run NH_3 adsorption isotherm was measured at 298 K at first by a commercial volumetric equipment (Autosorb-1, YUASA Co. Ltd.) after evacuating the catalyst at an appropriate temperature between 393–573 K for 2 h. After evacuating the NH_3-adsorbed catalyst at 298 K for 3 h, the same catalyst was subjected to a second run NH_3 adsorption measurement at 298 K. The equilibrium time for every measuring point was 2 min. The irreversible NH_3 adsorption amount was obtained by the difference of the first- and the second-run adsorption isotherms. In the dynamic pulse injection measurement, a portion of NH_3 gas with a standard volume of 1.776 ml (at 293 K and 101 kPa) was introduced every 20 min into a He stream having a flow rate of 20 ml/min, which passes through a catalyst bed whose temperature was maintained at 373 K. An amount of 0.05 g of catalyst was used every time and was subjected to dehydration in a He flow at least for 2 h at 473 or 573 K prior to NH_3 pulse injection measurement. The NH_3 pulse adsorption amount was obtained by comparing the NH_3 pulse area monitored as $m/e = 16$ by a Q-MASS analyzer (MMC-200, ULVAC Co. Ltd.) up to the fifth time with the standard NH_3 gas pulse area.

After the pulse NH_3 adsorption with the same procedure as described above, the NH_3-adsorbed H-Hol was maintained in He stream or switched into a mixing stream of He + 10% O_2 or He + 10% NO having the same flow rate of 20 ml/min, and then a temperature programmed desorption (TPD) was started at a ramp rate of 10 K/min from 373 to 1073 K. Signals of $m/e = 16$, 32, 18, 28, 44 which are the characteristics of NH_3, O_2, H_2O, N_2, and N_2O, respectively, in the degas stream were collected by a Q-MASS analyzer (MMC-200, ULVAC Co. Ltd.).

2.3. NH_3 pulse reaction

After dehydration in He stream at 473 or 573 K for 2 h, the catalyst bed with temperature maintained was switched into a He + 10% NO stream having a flow rate of 20 ml/min. After stabilization of gas stream, a pulse of NH_3 (99.999% purify) with a volume of 1.776 ml (at 293 K and 101 kPa) was introduced every 10 min up to 15 times, and reaction is in progress at every pulse introduction. Signals of $m/e = 16$, 30, 28, 44 which are the characteristics of NH_3, NO, N_2, and N_2O, respectively, in the outlet gas stream were monitored by a Q-MASS analyzer (MMC-200, ULVAC

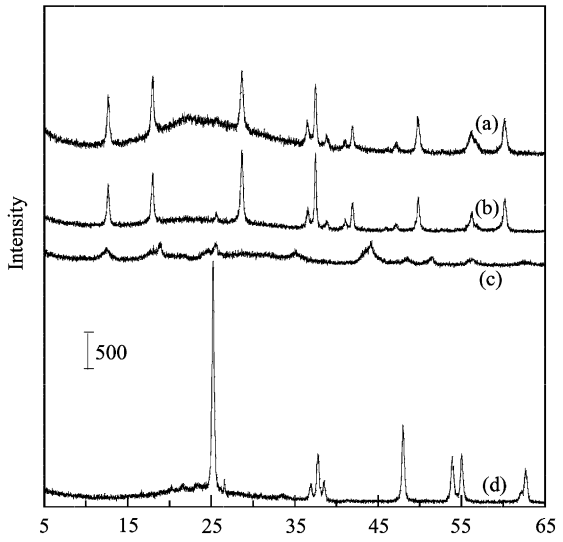

Fig. 1. XRD patterns of (a) H-Hol, (b) K-Hol, (c) HMnO, and (d) VTiO.

Co. Ltd.). The changes of the consumed NH_3 and NO amounts and the produced N_2 and N_2O amounts were calculated from the calibration curve of each pure gas, which has a correlation coefficient above 99.9%.

3. Results and discussion

3.1. Catalyst characterization and NH_3 adsorption

Fig. 1 shows the X-ray diffraction patterns (XRD) of the catalysts. H-Hol and K-Hol have the right crystal structures, similar to the natural cryptomelane-type [16]. The diffraction peaks of HMnO show the mixed properties of several crystal structures (spinel, α-MnO_2, γ-MnO_2, MgO), but less intense and very broad, indicating that HMnO is less crystalline due to a long time acid treatment. VTiO reveals the sharp diffraction peaks at 25.3, 37–39, 48.1, 53–56, and 62.7° due to the anatase support. A slight sharp peak at 26.6° shows the presence of crystalline V_2O_5 particles on TiO_2. The nitrogen adsorption isotherms at 77 K on all the catalysts are of typical type-II shapes, indicating the multi-layer adsorption properties. A greater hysteresis was observed on the desorption branch of N_2 on HMnO, indicating a partially mesoporous property of HMnO. The specific adsorption areas of the catalysts were calculated by Brunauer–Emmett–Teller (BET) method; the values are shown in Table 1. H-Hol, K-Hol and VTiO have small surface areas with values of 60–70 m^2/g. Although, H-Hol shows a larger surface area for NH_3 and H_2O adsorption [5], its surface area from N_2 adsorption is smaller due to exclusion of N_2 form the tunnel structure. On the other hand, HMnO has a large surface area, which should be arisen from a large amount of aggregates of tiny crystalline particles. Fig. 2 shows the comparison of TG/DTA curves of the catalysts. In comparison with the H-type manganese oxides, VTiO has only a slight dehydration without any peculiar DTA peak below 900 K. A great dehydration below 473 K and a corresponding endothermic peak at around 360 K are observed for HMnO. The dehydration behavior of HMnO is similar to those of zeolites [12,17], indicating that a large amount of H^+ sites, which can strongly retain water, are present in the surface of HMnO. K-Hol also has a gradual dehydration until 800 K, indicating that there exist also a part of H^+ sites in K-Hol.

Fig. 3 shows the comparison of first-, second-, and irreversible adsorption isotherms of NH_3 on various catalysts. Both physical and irreversible NH_3 adsorptions on H-Hol decrease with the increase of dehydration degree. Although, HMnO has a large amount of physical adsorption toward NH_3, its irreversible NH_3 adsorption amount is comparable with that of H-Hol

Table 1
Specific surface areas (SSA), NH_3 static irreversible ($n_{NH_3,s}$) and dynamic pulse adsorption ($n_{NH_3,d}$) amounts of the catalysts

Catalyst	Dehydration temperature (K)	SSA (m^2/g)	$n_{NH_3,s}$ (mmol/g)	$n_{NH_3,d}$ (mmol/g)
H-Hol	473	70	1.27	0.36
H-Hol	573	70	0.39	0.17
K-Hol	473	65	0.59	0.43
HMnO	473	209	1.38	0.73
VTiO	473	60	0.23	0.17

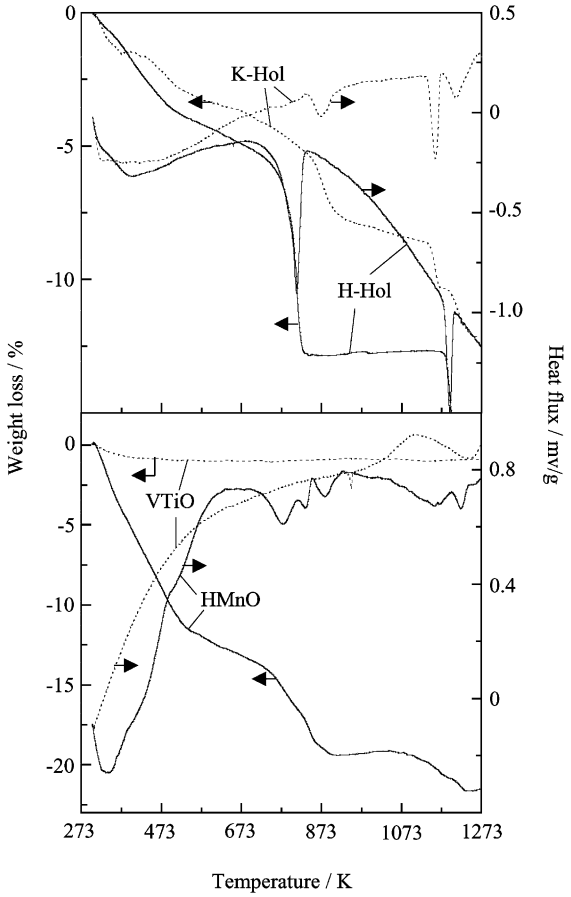

Fig. 2. TG/DTA curves of H-Hol, K-Hol, HMnO, and VTiO.

dehydrated at 473 K. NH_3 adsorption on K-Hol and VTiO are lower than those on H-type catalysts; their physical NH_3 adsorptions are comparable with each other, but the irreversible NH_3 adsorption on VTiO is less than that on K-Hol. Table 1 also shows the comparison of irreversible NH_3 adsorption from the static volumetric measurement and the pulse NH_3 injection measurement on various catalysts. The irreversible NH_3 adsorption amounts from the static volumetric method are greater than those from the pulse adsorption method, indicative of a rate-determining process for NH_3 adsorption. Especially, the sequence of irreversible NH_3 adsorption amounts from the static volumetric method is not in parallel with those from pulse adsorption method for H-Hol, indicating that the energy barrier for NH_3 adsorption into the tunnel of H-Hol are much higher.

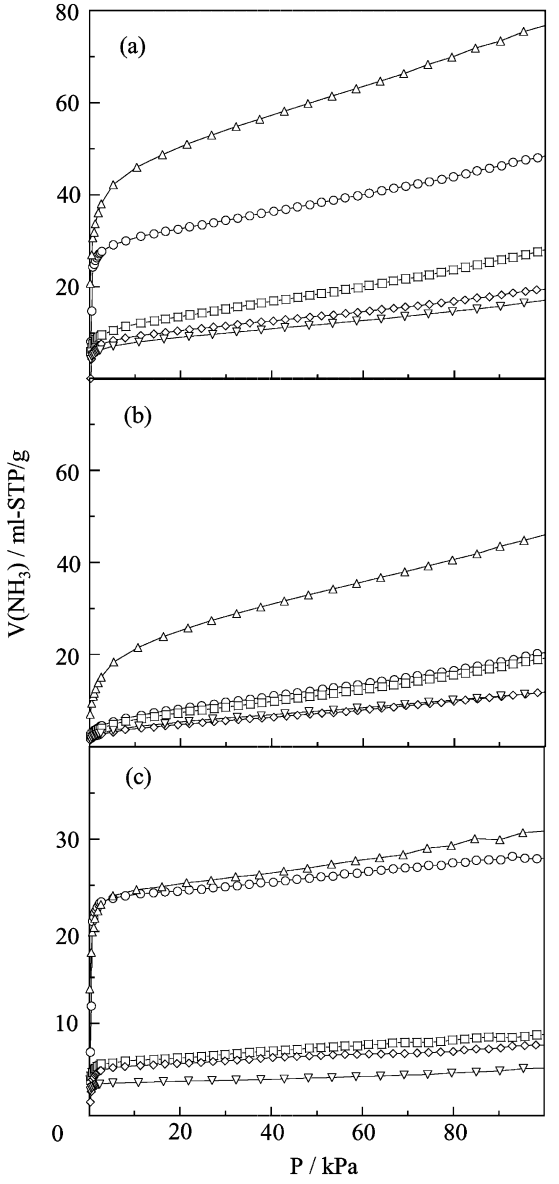

Fig. 3. Comparison of (a) first run, (b) second run, and (c) irreversible NH_3 adsorption isotherms on H-Hol after evacuation at 473 K (○) and 573 K (□). K-Hol (◇), HMnO (△), and VTiO (▽) after evacuation at 473 K.

3.2. Desorption and decomposition of NH_3 from NH_3-adsorbed H-Hol under various gas atmosphere

Fig. 4 shows the signals of desorption gases from NH_3-adsorbed H-Hol on increasing temperature under

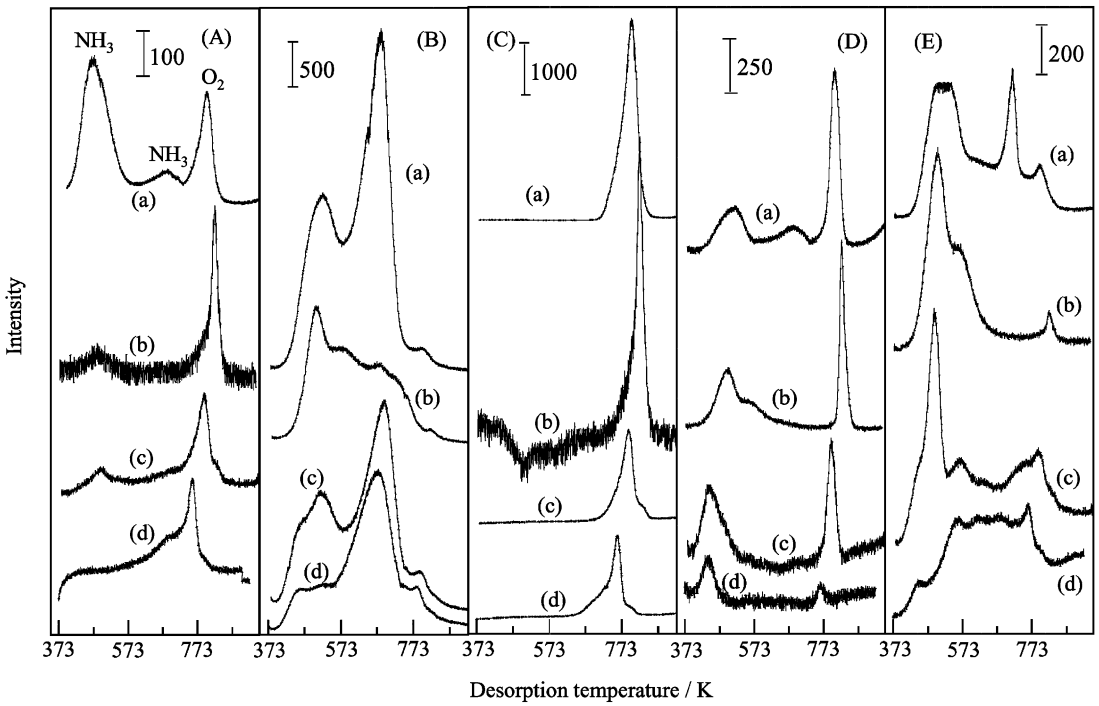

Fig. 4. Desorption gases from NH_3-adsorbed H-Hol on increasing temperature under atmosphere of (a) He, (b) He + 10% O_2, (c) He + 10% NO after evacuation at 393 K for adsorption, and (d) He + 10% NO after evacuation at 473 K for adsorption. (A) *m/e* = 16, (B) *m/e* = 18, (C) *m/e* = 32, (D) *m/e* = 28, and (E) *m/e* = 44.

atmosphere of He, He + 10% O_2, and He + 10% NO. As the peaks of *m/e* = 16 in (A) at higher temperature (around 773 K) are exactly the same position and the same peak shape with those of *m/e* = 32 in (C), these peaks are ascribed to the evolved oxygen gas. The peaks of *m/e* = 16 in (A) at the lower temperature (<700 K) are ascribed to the evolved ammonia gas because of no any signals in the corresponding positions of *m/e* = 32 in (C). The signals of *m/e* = 18, 28, and 44 are ascribed to the evolved H_2O, N_2, and N_2O, respectively, because of no other impurities such as CO or CO_2 in the evolved gases. Desorption under atmosphere of He gives two reversible NH_3 evolution peaks: a large peak at 473 K and a slight peak at 673 K. These two NH_3 evolution peaks are arisen from two adsorbed $–NH_4^+$ species with the corresponding IR band (–NH deformation) at 1400 and 1424 cm^{-1}, respectively [5,21]. Another FT-IR result indicates that the $–NH_4^+$ species with IR band at 1424 cm^{-1} are less amount and mainly present on H-Hol pre-evacuated above 573 K [21]. Furthermore, the surface sites to form these $–NH_4^+$ species are unstable and gradually transformed to Lewis acid sites on repeating NH_3 adsorption/desorption [21]. Thus, the H^+ sites on H-Hol, which form these $–NH_4^+$ species, are of reactive properties. Actually, H_2O, N_2, and N_2O are evolved at the same positions for the two NH_3 evolution peaks, indicating that one part of $–NH_4^+$ adspecies, especially the $–NH_4^+$ adspecies releasing NH_3 at a higher temperature are oxidized by surface oxygen following the reactions below:

$$4[–NH_4^+]_1 + 9[O^{2-}]_1 + 14[Mn^{4+}] \rightarrow N_2 + N_2O + 8H_2O + 14[Mn^{3+}] \quad (473\,K) \quad (1)$$

$$4[–NH_4^+]_2 + 9[O^{2-}]_2 + 14[Mn^{4+}] \rightarrow N_2 + N_2O + 8H_2O + 14[Mn^{3+}] \quad (673\,K) \quad (2)$$

The above reactions bring about partial reduction/rearrangement of the surface of H-Hol, but less influence on the change in the bulk crystal structure,

which is stable until 673 K (Fig. 2). At a higher temperature (780 K) corresponding to the structural transformation of H-Hol (α-MnO_2) to Mn_2O_3, oxygen desorbs together with a large signal of N_2 and a slight signal of N_2O, indicating that large amount of nitrogen atoms originated from the NH_3 adspecies are accommodated on H-Hol either in a form of more oxidized adspecies such as nitrate species or in a form of direct bonding with the lattice Mn(O) ions [13,18–20] on increasing desorption temperature. Increasing temperature under atmosphere of O_2 leads to the disappearance or less intensity of N_2, N_2O, and H_2O peaks evolved from reaction (2) and a much less intensity in the irreversible NH_3 peak, but a larger N_2 and N_2O evolutions at 473 K. It is, thus, followed that the presence of gaseous oxygen stabilizes the $[O^{2-}]_2$ sites, while accelerate the reaction of $-NH_4^+$ adspecies with gaseous oxygen at the lower temperature. The effect of gaseous oxygen to stabilize the bulk crystal structure is also evident because the O_2 evolution peak due to the structural transformation shifts to a higher temperature side. The N_2 and N_2O peaks are also observed at the temperature at which the structural transformation occurs, indicating that nitrogen atoms can also be retained up to a higher temperature in the oxygen atmosphere.

On the other hand, increasing temperature under atmosphere of NO (curve (c)) further accelerates the oxidation of $-NH_4^+$ species on $[O^{2-}]_1$, giving only a slight reversible NH_3 peak at 473 K and a much larger N_2 and N_2O peaks at the same temperature. Desorption of H_2O at around 680 K is also observed, indicating that reaction of $-NH_4^+$ adspecies and NO is also in progress in the vicinity of $[O^{2-}]_2$ sites. However, there is no correspondent N_2 and N_2O evolution at around 680 K. Furthermore, while the evolved O_2 and N_2 peaks at 780 K, where the structural transformation occurs, becomes less intensity, the evolved N_2O peak is greatly enhanced. These phenomena manifest that the reaction of $-NH_4^+$ species and NO on $[O^{2-}]_2$ sites results in the production of a larger amount of nitrogen-containing deposits which are decomposed at the temperature of the structural transformation and evolved mainly in a form of N_2O instead of N_2 and O_2. Pre-dehydration of H-Hol at 473 K (curve (d)) brings about a larger amount of N_2 evolution instead of H_2O and N_2O evolution below 473 K and a much slighter N_2 evolution at 773 K, where the structural transformation occurs. Larger portion of H_2O desorbs at a higher temperature (573–700 K) together with an enhanced broad peak of N_2O. The presence of NO stabilizes nothing, but accelerates the collapse of the crystal structure of hollandite as can be seen from the lower temperature shifting for the structural transformation. These facts indicate that the presence of NO induces the oxidation reaction between NO and NH_3-adsorbed H-Hol.

3.3. Pulse reaction of NH_3 in He + 10% NO stream

In order to further examine, the low temperature oxidizing property of NH_3 in NO atmosphere as manifested by the above TPD result, a pulse of NH_3 was introduced into the He + 10% NO stream which passes through the dehydrated H-Hol without NH_3 adsorption in a quartz reactor. Fig. 5 shows the signals of the produced N_2 and N_2O every pulse number on H-Hol in comparison with those on K-Hol, HMnO, VTiO, and the blank. While only N_2 is produced on VTiO, indicative of its excellent selectivity, both N_2 and N_2O are formed on all the manganese oxides. Production of N_2 and N_2O for all the catalysts decreases with the increase of the pulse number, becoming constant after pulse number eight. The decrease in N_2O production with the increase of the pulse number on manganese oxides are more evident than the decrease in N_2 production, indicating that the surface active sites such as surface active oxygen species may participate in the gas phase reaction. Every pulse reaction gradually leads to the loss or the deactivation (by surface deposit formation) of the surface active oxygen species, i.e. the loss of surface oxidation ability, thus, resulting in a gradual decrease in N_2O as well as N_2 productions. Table 2 shows the amounts of the consumed NH_3 and NO, and the produced N_2 and N_2O on all the catalysts. While the initial NH_3 conversion is 59% for VTiO, those for the manganese oxides are >99%. Irrespective of a large surface area (from N_2 adsorption), HMnO has the similar N_2 and N_2O productions with that on H-Hol pre-dehydrated at 473 K, indicating that only the strong H^+ sites have responsibility for catalytic formation of N_2 and N_2O. Dehydration of H-Hol at 573 K gives the highest N_2O production at the initial pulse reaction, but the highest N_2 production after the eighth pulse reaction, indicating the important role of the dehydrated sites in N_2 and

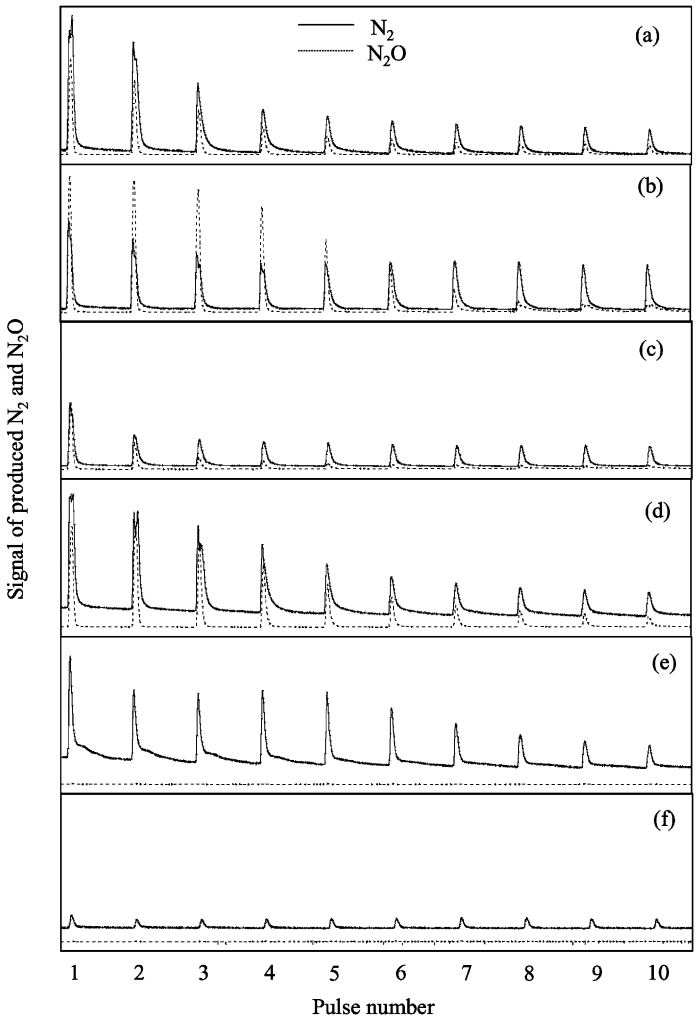

Fig. 5. N_2 and N_2O production from pulse reaction of NH_3 in He + 10% NO stream on (a) H-Hol after dehydration at 473 K, (b) H-Hol after dehydration at 573 K, (c) K-Hol, (d) HMnO, (e) VTiO, and (f) in empty sample cell. Reaction temperature: (a) and (c)–(f), 473 K; (b), 573 K.

N_2O formation. Taking into account the chemically stoichiometric ratio of 2 {[N_2 production] + [N_2O production]}/[NH_3 consumed], one can hardly ascribe a definite reaction described below to the reaction of NH_3 and NO on the manganese oxides:

$$2NH_3 + 2NO + 2[O^{2-}] + 4[Mn^{4+}] \rightarrow N_2 + N_2O + 3H_2O + 4[Mn^{3+}] \quad (3)$$

$$2NH_3 + 4NO \rightarrow 2N_2 + N_2O + 3H_2O \quad (4)$$

Furthermore, the consumed NO amounts are larger than those required by any chemically stoichiometric equations to form N_2 and N_2O, indicating that other forms of NO_x should be also produced. We confirmed that an enhanced NO_2 ($m/e = 46$) production occurs at the pulse reactions of the first several pulse numbers for H-Hol dehydrated at 573 K, while an intense desorption peak of NO_2 was observed for K-Hol during TPD experiment in He after the pulse reaction. These results reveal that both NO_2 and the surface deposits

Table 2
The amounts of the consumed NH_3 (ΔNH_3) and NO (ΔNO) and the produced N_2 (ΔN_2) and N_2O (ΔN_2O), the NH_3 conversion (x), and the ratios of 2 {[N_2 production] + [N_2O production]}/[NH_3 consumed] (α) of the initial and the tenth pulse reaction[a]

Catalyst	Pulse no. 1 (mmol/g)					Pulse no. 10 (mmol/g)				
	ΔNH_3 (x)	ΔNO	ΔN_2	ΔN_2O	α	ΔNH_3 (x)	ΔNO	ΔN_2	ΔN_2O	α
H-Hol-473	1.7 (99%)	6.4	0.7	0.5	2.4	0.4 (22%)	1.2	0.09	0.07	0.9
H-Hol-573	1.7 (99%)	4.7	0.4	0.7	1.2	1.0 (61%)	2.7	0.20	0.15	0.7
K-Hol-473	1.7 (99%)	0.8	0.3	0.4	0.7	1.1 (68%)	0	0.07	0.02	0.2
HMnO-473	1.8 (100%)	6.9	0.6	0.6	1.3	0.7 (46%)	2.3	0.14	0.09	0.6
VTiO-473	0.9 (59%)	2.4	0.5	0	1.1	0.1 (6%)	0.3	0.09	0	2

[a] The values after the catalyst name denotes the dehydration and reaction temperature.

involving nitrogen atoms (e.g. nitrate-like species) are formed due to a stronger oxidizing ability of hollandite surface. Thus, formation of N_2 on manganese oxides should be a more complicated process. The above results definitely show that H-Hol has a capability to catalytically oxidize NH_3 under existence of NO.

4. Conclusion

H-Hol has a comparable amount of strong H^+ sites with the high surface area manganese oxide, which have relationship with NH_3 decomposition. In a reducing atmosphere, reaction of the adsorbed NH_3 with the surface active oxygen species on H-Hol is accelerated on increasing temperature, leading to a partial oxidation of NH_3 at lower temperatures and a great release of N_2 at the temperature of structural transformation. The presence of O_2 induces the decomposition of NH_3 from NH_3-adsorbed on H-Hol at the lowest temperature and has an effect to stabilize the crystal structure of H-Hol on increasing temperature. The presence of NO enhances N_2 production at a lower temperature and the oxidizing reaction with H-Hol on increasing temperature. H-Hol has the greatest N_2 production, but less selectivity to form N_2 in an $NH_3 + NO$ pulse reaction condition in comparison with the high surface area manganese oxide and the commercial de-NO_x catalyst.

References

[1] R.N. De Guzman, Y. Shen, B.R. Shaw, S.L. Suib, C. O'Young, Chem. Mater. 5 (1993) 1395.
[2] S. Bach, J.P. Pereira-Ramos, N. Baffier, Solid State Ionics 80 (1995) 151.
[3] S.L. Brock, N. Duan, Z. Tian, O. Giraldo, H. Zhou, S.L. Suib, Chem. Mater. 10 (1998) 2619.
[4] Q. Feng, H. Kanoh, K. Ooi, J. Mater. Chem. 9 (1999) 319.
[5] Z.-M. Wang, S. Tezuka, H. Kanoh, Chem. Lett. (2000) 560.
[6] Q. Feng, H. Kanoh, Y. Miyai, K. Ooi, Chem. Mater. 7 (1995) 148.
[7] M. Tsuji, M. Abe, Solv. Ext. Ion Exch. 2 (1984) 253.
[8] Y. Tanaka, J. Porous Mater. 2 (1995) 135.
[9] B. Dhandapani, S.T. Oyama, Chem. Lett. (1995) 413.
[10] W.S. Kijlstra, D.D. Brands, E.K. Poels, A. Bliek, J. Catal. 171 (1997) 208.
[11] L.S. Singoredjo, R.B. Korver, F. Kapteijn, J.A. Moulijn, Appl. Catal. B: Environ. 1 (1992) 297.
[12] Z.-M. Wang, H. Kanoh, Thermochim. Acta., in press.
[13] S. Tezuka, Z.-M. Wang, K. Ooi, H. Kanoh, in: D.D. Do (Ed.), Adsorption Science and Technology, World Scientific, Singapore, 2000, p. 319.
[14] Y. Miyai, K. Ooi, S. Katoh, J. Colloid Interface Sci. 130 (1989) 535.
[15] Y. Miyai, K. Ooi, S. Katoh, Sep. Sci. Technol. 23 (1988) 179.
[16] JCPDS-ICDD Powder Diffraction File no. 20-908.
[17] D.W. Breck, Zeolite Molecular Sieves — Structure, Chemistry, and Use, Wiley/Interscience, New York, 1974.
[18] H. Berndt, K. Büker, A. Martin, A. Brückner, B. Lücke, J. Chem. Soc., Faraday Trans. 91 (1995) 725.
[19] S. Kittaka, T. Hamaguti, T. Umezu, T. Endoh, T. Takenaka, Langmuir 13 (1997) 1352.
[20] L. Pascual, A. Durán, Mater. Res. Bull. 31 (1996) 77.
[21] Z.-M. Wang, S. Tezuka, H. Kanoh, Chem. Mater. 13 (2001) 530.